

New Bayesian algorithm for sea ice detection with QuikSCAT

Maria Belmonte Rivas, Ad Stoffelen

Abstract— We propose a sea ice detection method for a rotating Ku-band scatterometer with dual-polarization capability such as Seawinds on QuikSCAT based on probabilistic distances to ocean wind and sea ice Geophysical Model Functions (GMFs), and evaluate its performance against existing active and passive microwave methods. All these algorithms yield similar results during the ice growth season, but show substantial differences during the spring and summer months. A dedicated comparison against high resolution SAR and optical imagery shows that major discrepancies relate to newly formed, low concentration and water saturated sea ice species. The new GMF based algorithm for sea ice detection with Seawinds on QuikSCAT improves on the misclassification scores that affect previous algorithms and provides daily sea ice masks at 25 km resolution for use in ground processors that require the effective removal of sea ice contaminated pixels.

Index Terms— Sea ice, Bayes procedures, microwave reflectometry, microwave radiometry.

I. INTRODUCTION

IN 2007, the summer extent of Arctic sea ice observed by satellite sensors reached its lowest value on record since 1979 [1]. Satellite platforms provide a convenient way to monitor the vast expanses of sea ice in the Polar Regions, mainly thanks to microwave sensors which, contrary to optical techniques, can operate at night and in all-weather conditions. The determination of sea ice extents from satellite platforms is exploited as a marker for climate change, a navigation aid and a validation tool in cryospheric modelling studies. Sea ice detection is routinely performed by two types of sensors: passive microwave radiometers, which observe the natural emissions of the Earth's surface [2], and active microwave scatterometers, which collect the energy reflected from an initially transmitted pulse ([3],[4],[5]). Earlier studies have shown a reasonable agreement between scatterometer and radiometer sea ice extents [6] with remarkable seasonal discrepancies characterized by negatively biased scatterometer extents during the sea ice growth season [7] and negatively biased radiometer extents during the summer months [8]. In this paper, we revisit the determination of sea ice extents using satellite microwave sensors, propose an improved method for sea ice detection using the SeaWinds scatterometer on QuikSCAT and evaluate its performance against existing

active and passive microwave algorithms across the sea ice growth and melt cycles.

Section II details the construction and underlying principles of the Geophysical Model Function (GMF) based sea ice detection method for QuikSCAT. In Section III, we examine the location of the resulting sea ice edge against the sea ice concentration from the AMSR-E Enhanced NASA Team (NT2) algorithm and the QuikSCAT Scatterometer Climate Record (SCP). The extent and nature of the discrepancies observed are further analyzed using higher resolution optical and synthetic aperture radar (SAR) data. Section IV summarizes our results and concludes with some notes on future work.

II. ALGORITHM DESCRIPTION

Scatterometers are active microwave sensors whose primary mission consists in the determination of surface winds over the oceans. The QuikSCAT scatterometer radiates microwave pulses at a frequency of 13.4 GHz and employs a rotating dish antenna for the reception of horizontally and vertically polarized returns from a variety of incidence and azimuth angles, providing a diversity of views that allows for the detection of the wind signature over the ocean (Fig.1).

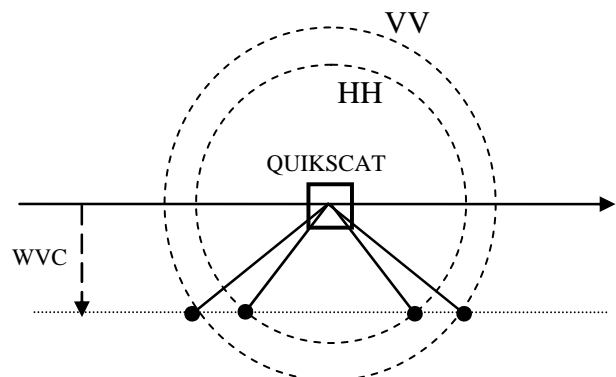


Fig. 1. Top view of QuikSCAT observation geometry. The sensor provides a total of $N = 4$ backscatter views per Wind Vector Cell (WVC). The incidence angles for the inner HH and outer VV polarized beams are 46 and 54 degrees respectively.

An inspection of the distribution of backscatter points from ocean and sea ice surfaces in the QuikSCAT backscatter space $\{\sigma_{HH\text{-fore}}^0, \sigma_{VV\text{-fore}}^0, \sigma_{VV\text{-aft}}^0, \sigma_{HH\text{-aft}}^0\}$ reveals that they occupy largely distinct sectors (see Fig.2). While surface scattering from a wind roughened ocean is characterized by azimuthal (fore/aft) anisotropy and a certain degree of polarization,

volume scattering from a sea ice slab results in isotropic, depolarized and generally stronger returns. The first sea ice detection algorithms with scatterometer data relied on hard-threshold tests that capitalized on these properties. They evolved in time into maximum likelihood (also known as Bayesian) methods with separate class cluster centroids for mean backscatter (σ_{HH}), polarization ratio (σ_{VV}/σ_{HH}) and azimuthal anisotropy ($\Delta\sigma_{HH}, \Delta\sigma_{VV}$) acting as discriminant parameters, and jointly Gaussian [3] or empirically adjusted covariances [4] characterizing the dispersion of the discriminants about the class centroids. The new GMF-based approach reverts the classification back to the measurement space by replacing the former class centroids for mean backscatter, polarization and anisotropy by extended Geophysical Model Functions (GMFs) for ocean wind and sea ice backscatter at Ku-band [9]. The advantage of this approach is that the dispersion of measurements about extended GMFs is smaller than that about cluster centroids, actually approaching the limit imposed by the scatterometer receiver noise and allowing the Bayesian method to reach its full discrimination power.

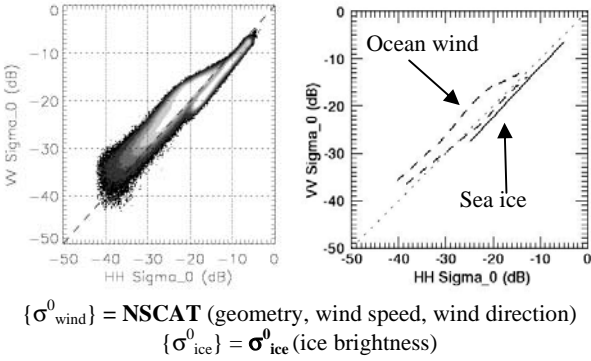


Fig. 2. Observed distributions of backscatter data (LEFT) and empirical ocean wind and sea ice model functions (RIGHT) in the space of QuikSCAT measurements

The empirical GMF for ocean wind σ_{wind}^0 is the same applied to retrieve wind vectors over ocean surfaces operationally. It was determined on the basis of a statistical comparison between ADEOS NSCAT 14 GHz dual-polarized backscatter measurements and collocated ECMWF NWP winds [10]. The empirical GMF for sea ice σ_{ice}^0 is drawn from the observed distribution of pure (100% concentration) winter sea ice backscatter [11], which neatly groups along a straight curve in the QuikSCAT dB-space and can be simply expressed as $\sigma_{VV, dB} = 1.06 \cdot \sigma_{HH, dB} - 1.0$ on (see Fig.2).

The GMF-based algorithm computes the minimum squared distances (or maximum likelihood estimators, MLE) to the ocean wind σ_{wind}^0 and sea ice σ_{ice}^0 model functions as:

$$MLE_{wind} = \sum_{i=1, \dots, N} (\sigma_i^0 - \sigma_{wind,i}^0)^2 / \text{var}[\sigma_{wind}^0] \quad (1)$$

$$MLE_{ice} = \sum_{i=1, \dots, N} (\sigma_i^0 - \sigma_{ice,i}^0)^2 / \text{var}[\sigma_{ice}^0] \quad (2)$$

where i is an index to the components of the backscatter vector and N is its dimension (or number of views per cell, N

= 4 for QuikSCAT) and the normalizing factors $\text{var}[\sigma_{class}^0]$ guarantee that the variance of backscatter components about the corresponding model function is unity. The variance of measurements about the ocean GMF is a well known parameter and expressed as the sum of instrumental K_p and geophysical K_{geo} random gaussian components as:

$$\text{var}(\sigma_{wind}^0) = (K_p^2 + K_{geo}^2)(\sigma_{wind}^0)^2 \quad (3)$$

The instrumental K_p noise refers to radiometric uncertainty in the SeaWinds receiver chain [12] with a best case value of 10% at high winds. The geophysical K_{geo} noise is a lumped concept that accounts for perturbations in ocean backscatter due to non-instrumental causes such as wind variability, atmospheric instability or undetected rain ([13],[14]) with a best case value of 5% at high winds. The variance of pure (100% concentration) sea ice backscatter about the sea ice GMF can be attributed to instrumental K_p noise alone, although we introduce a tolerance factor α to make allowance for larger excursions caused by mixed ocean/ice conditions:

$$\text{var}(\sigma_{ice}^0) = \alpha^2 K_p^2 (\sigma_{ice}^0)^2 \quad (4)$$

The value of α is adjusted empirically using independent data. Observe that minimum squared distances MLE are defined as the sum of N squared normal standard variables. Consider that backscatter excursions that lie parallel to the GMFs cannot contribute to MLE, to infer that the expected distribution of MLEs to the ocean (2D) and sea ice (1D) model functions can be approximated by chi-square distributions with $N-2$ and $N-1$ independent degrees of freedom:

$$p(MLE_{ice}) = \sqrt{\frac{MLE_{ice}}{2\pi}} \exp(-MLE_{ice}/2) \quad (5)$$

$$p(MLE_{wind}) = \frac{1}{2} \exp(-MLE_{wind}/2) \quad (6)$$

The observed and expected MLE distributions to the SeaWinds ocean and sea ice GMFs are displayed in Fig.3.

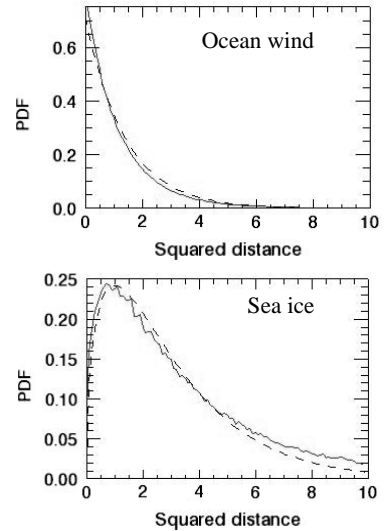


Fig. 3. Observed (continuous) and expected (dashed) MLE distributions to ocean wind (TOP) and winter sea ice (BOTTOM) model functions. For reference, the instrumental noise standard deviation is about 0.5 dB ($\alpha = 1$, $K_p \sim 10\%$) over most of QuikSCAT dynamic range.

Once we know the mean location and expected dispersion of

the sea ice and ocean backscatter populations in the QuikSCAT measurement space, we can proceed to establish a Bayesian decision rule. The Bayesian posterior sea ice probability is formulated as:

$$p(ice | \sigma^0) = \frac{p(\sigma^0 | ice)p_0(ice)}{p(\sigma^0 | ice)p_0(ice) + p(\sigma^0 | wind)p_0(wind)} \quad (7)$$

in terms of prior historic information $p_0(ice)$ and $p_0(wind)$, and the conditional probability distributions of minimum squared distances $p(\sigma^0 | wind)$ and $p(\sigma^0 | ice)$ to sea ice and ocean model functions. An important weakness of this method concerns the loss of discrimination power at locations where class GMFs approach one another. That is to say, bright multiyear ice and large ocean wind speeds share similar backscatter signatures. To address this problem, we introduce an external weight that inhibits large differences between apparent surface winds v and Numerical Weather Prediction wind forecasts v_{NWP} in ice contaminated conditions:

$$p(\sigma^0 | ice) = p(MLE_{ice})$$

$$p(\sigma^0 | wind) = p(MLE_{wind}) \cdot \exp(-|\bar{v} - \bar{v}_{NWP}|^2 / 2\Delta v^2) \quad (8)$$

where $\Delta v = 5$ m/s with ECMWF 3-hourly wind forecasts. This correction prevents bright ice from being interpreted as a strong wind at high latitudes, but it has little effect elsewhere. The prior sea ice and ocean wind probabilities are set initially to $p_0(ice) = 0.50 = 1 - p_0(wind)$, updated every orbit as $p_0(ice) = p(ice | \sigma^0)$ and relaxed daily as:

$$p_0(ice) = \begin{cases} 0.50 & \text{if } p(ice | \sigma^0) > 0.30 \\ 0.15 & \text{if } p(ice | \sigma^0) < 0.30 \end{cases} \quad (9)$$

These settings have been chosen to maximize the quality of the prior information used for sea ice detection. The Bayesian algorithm implemented at KNMI generates near-real time daily sea ice masks with NRT QuikSCAT L2B BUFR data [15] using a 55% threshold to posterior sea ice probabilities in Eq.(7). The sea ice masks are filled with backscatter strength values indicative of ice type/age (Fig. 4) and archived.

III. ALGORITHM VALIDATION

We start by comparing the sea ice extents derived from the QuikSCAT GMF based algorithm against passive microwave estimates during a whole year beginning Sep'06. The passive microwave sea ice extents result from applying a 15% threshold on daily AMSR-E sea ice concentrations generated by the Enhanced NASA Team (NT2) algorithm (AE SI12 V.001, [16],[17],[18]). The wintertime location of the AMSR-NT2 15% concentration edge has been successfully validated against RADARSAT SAR and MODIS imagery [21], but its accuracy reduces drastically during the summer months due to weather effects, unresolved ice types and surface melt effects [16]. To illustrate the sensitivity of our new method to the expected dispersion of backscatter about the sea ice model, the GMF based algorithm is run using different tolerance factors ($\alpha=1, 2$ and 3 in Eq.(4) with $\text{std}[\sigma^0_{ice}] = 0.5, 1.0$ and 1.5 dB) and the results are shown in Figure 5. The comparison is performed on 12.5 km polar stereographic grids using a common landmask with a 25 km coastal filter. Note that the total extent of sea ice detected by QuikSCAT increases with the expected sea ice model variance, and that this effect can be

attributed to the algorithm sensitivity to mixed ice/ocean pixels, i.e. pixels with mixed surface and volume backscatter signatures.



Fig. 4. Arctic and Antarctic sea ice extents for May 15th 2007 from scatterometer (QSCAT-KNMI) with sea ice GMF noise $\text{std}[\sigma^0_{ice}] = 1.5$ dB. Background grey scale represents sea ice backscatter strength.

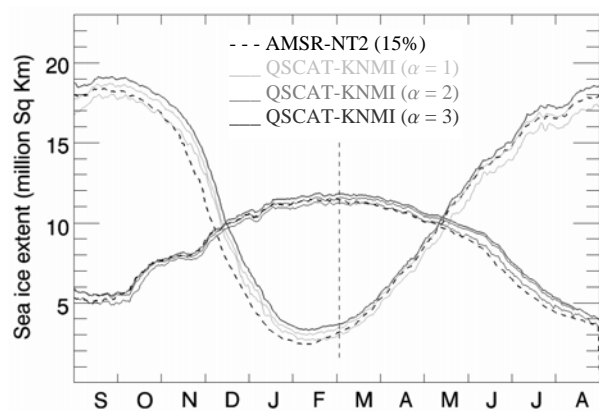


Fig. 5. Daily Arctic and Antarctic sea ice extents for Sep'06 to Sep'07 from radiometer (AMSR-NT2, dashed line) and scatterometer (QSCAT-KNMI, shaded lines) using different sea ice model variances.

Mixed ice/ocean pixels are the hardest to classify since they remain at comparably similar distances from the sea ice and ocean GMFs. They arise in different conditions including: i) low concentration and water saturated ice species that populate the Arctic margin during the melt season or the Antarctic edge all year round, ii) the partly translucent new ice formed during the growth season, and iii) all areas affected by moderate to heavy precipitation [19]. The mixed signature induced by rain cannot be distinguished from that of thin or low concentration sea ice in terms of backscatter alone, and constitutes our only source of misclassification noise. To increase the sensitivity of the QuikSCAT algorithm to thin and low concentration sea ice, the tolerance to mixed ice/ocean classes should be increased to the point where misclassification noise due to rain contamination becomes excessive. One such point is found at $\text{std}[\sigma_{\text{ice}}^0] = 1.5 \text{ dB}$ ($\alpha = 3$). The utilization of lower tolerance factors would improve the rain rejection properties of the algorithm, but also give way to defective scatterometer extents, particularly during the sea ice growth season (see ascending branches in Fig.5).

An additional source of validation are the QuikSCAT sea ice extents derived from the cluster centroid method [3], denoted QSCAT-SCP here (from the Scatterometer Climate Pathfinder record, Version 2).

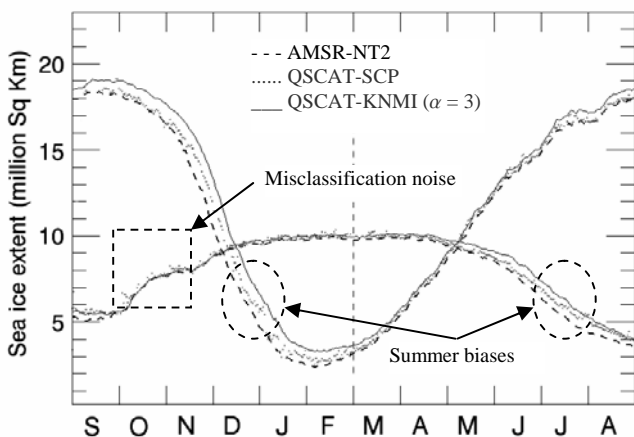


Fig. 6. Daily Arctic and Antarctic sea ice extents for Sep'06 to Sep'07 from radiometer (AMSR-NT2, dashed line) and scatterometer (QSCAT-KNMI 1.5 dB, continuous line and QSCAT-SIRF, dotted line)

Fig. 6 compares the QSCAT-SCP method against the AMSR-NT2 and QSCAT-KNMI algorithms between Sep'06 and Sep'07 to show good qualitative agreement during the sea ice growth season in both hemispheres, but large discrepancies as the melt season sets in. Also note that QSCAT-SCP is affected by a substantial amount of misclassification noise due to wind storm events near the ice edge, which manifest in Fig. 6 as a dispersion in daily areas during the Arctic fall and winter seasons. The mean daily AMSR-NT2 sea ice concentration along the QSCAT-SCP and QSCAT-KNMI ice edges provides further evidence of their relative performance. The mean wintertime sea ice concentration along the QSCAT-SCP edge stays about 25-30%, whereas the newer QSCAT-KNMI method reaches lower concentration values, down to 10-15%

with slightly worse performance during the dynamic Arctic fall season (Fig. 7). Other known problems of the QSCAT-SCP method are its poor detection of water openings within the ice pack (a.k.a. polynyas) and limited latitudinal extent. These problems have been addressed in later and improved versions of the cluster centroid method (see e.g. [4] or [20] with enhanced-resolution QuikSCAT data), but the average sea ice concentration at the ice edge remains the same as that reported here for QSCAT-SCP. The much lower sea ice concentration values observed at the edge in the summer months are indicative of defective radiometer estimates, an issue which will be explored next.

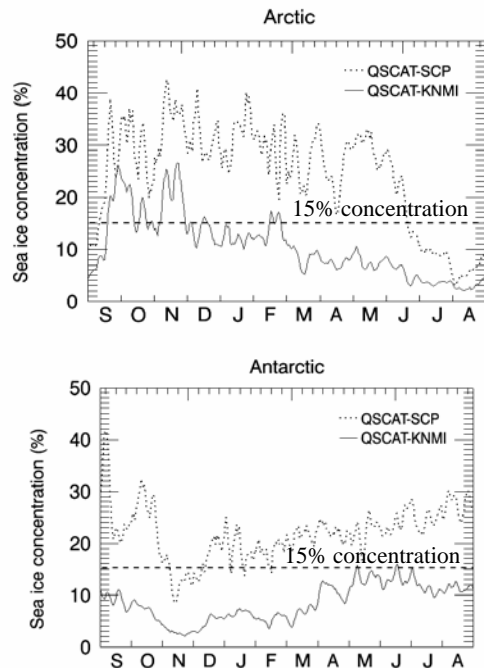


Fig. 7. Daily average AMSR-NT2 sea ice concentration along the QSCAT-SCP and QSCAT-KNMI ice/ocean boundaries over the Arctic (top) and Antarctic (bottom) regions from Sep'06 to Sep'07.

Having examined the quality and concordance between active microwave (AM) and passive microwave (PM) sea ice extents during the fall and winter seasons, we are left to evaluate their summertime discrepancies. We make use of high resolution MODIS (MOD29 from NSDIC DAAC, Version 5) [22] and ASAR Global Monitoring data (ASA_GM1_1P provided by ESA). We have inspected more than a hundred optical and radar images for algorithm validation at locations where different methods showed greater differences, and selected a few cases as representative of the most prevalent conditions (see Figs. 8 and 9). In general, the combined MODIS and ASAR records confirm that all the ice edge algorithms under study come to agree to within 25 km over areas that do not include mixed ice/ocean pixels (i.e. thin, low concentration or rotten sea ice). Figure 8A shows a typical detection discrepancy involving newly formed thin ice off the New Siberian Islands in the Arctic Sea. The QSCAT-SCP algorithm is missing a large tongue of new ice with dark smooth appearance in the image, which is however detected by both the QSCAT-KNMI and AMSR-NT2 algorithms.

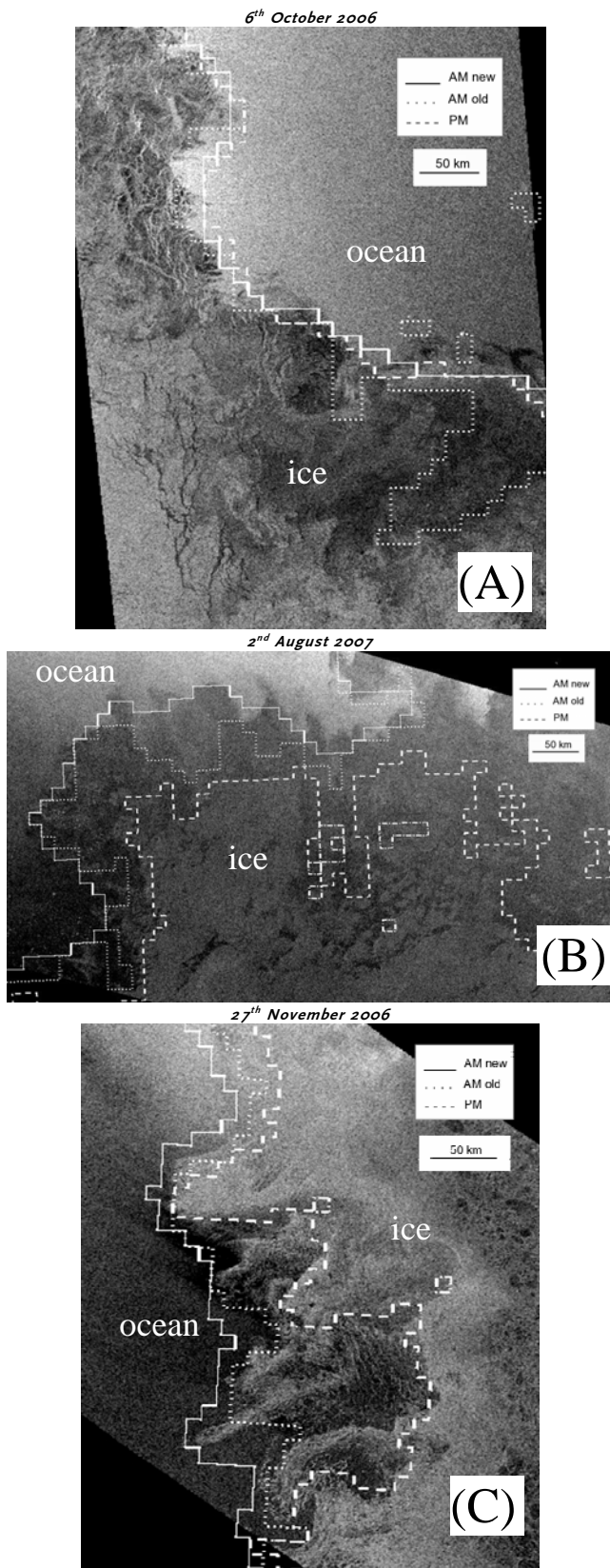


Fig. 8. Sea ice edge from QSCAT-KNMI (AM new, continuous line), QSCAT-SCP (AM old, dotted line) and AMSR-NT2 (PM, dashed line) on ASAR Global Monitoring backscatter data. Images are approximately 500 x 500 km wide.

Note that the presence of frequencies as high as 85GHz (i.e. lower penetration depths into sea ice) in passive microwave sensors plays favorable to thin ice detection during the ice growth season. Figure 8B shows a typical example of summer biases in the Beaufort Sea, featuring a large expanse of decaying and water saturated ice completely missed by the AMSR-NT2 algorithm. The QSCAT-SCP method can only detect it partially. Figure 8C provides another instance of summer biases along the ice edge in the Southern Ocean, this time featuring a number of ice bands of varying concentration. Low concentration, wave battered, decaying and water saturated ice are all examples of diffuse ice conditions most likely to pass undetected by passive microwave algorithms [23]. One last example is shown in Figure 9, taken from the MODIS sensor over the Baffin Bay and featuring a large but sparse floe field that passes undetected by both the AMSR-NT2 and QSCAT-SCP algorithms. The same scene is observed by MODIS in two sequential overpasses 1½ hour apart, but the floe field is mistaken for clouds in both cases. Up to this point, we have gained enough confidence to say that the performance of the GMF based Bayesian sea ice detection algorithm with QuikSCAT data remains unparalleled.

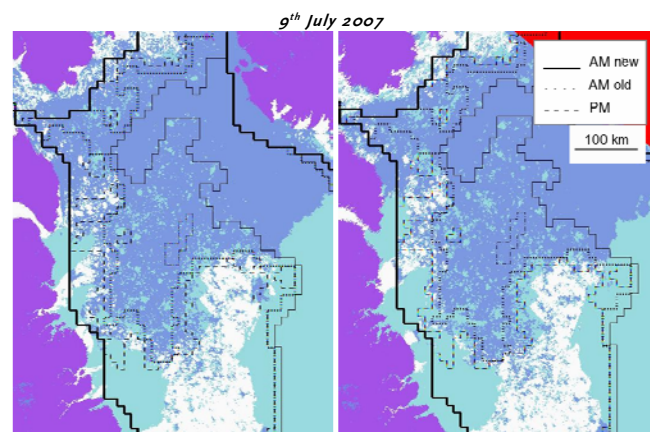


Fig. 9. Sea ice edge from QSCAT-KNMI (AM new, continuous line), QSCAT-SCP (AM old, dotted line) and AMSR-NT2 (PM, dashed line) on two sequential MODIS overpasses. MODIS products are cloud masked (cyan) and identify sea ice by its reflectance characteristics.

IV. CONCLUSIONS AND FUTURE WORK

This paper details the construction of an improved sea ice detection algorithm for the SeaWinds scatterometer on QuikSCAT that exploits detailed knowledge about the ocean wind and sea ice backscatter signatures at Ku-band. The improvement of the new algorithm over earlier scatterometer methods lies in its optimal utilization of the statistical distribution of backscatter in the space of measurements; in particular, the introduction of extended ocean and sea ice Geophysical Model Functions enhances dramatically the

discrimination power of the Bayesian approach. The performance of the new algorithm is validated against existing active and passive microwave sea ice detection algorithms on a global scale, and against high resolution optical and radar imagery on a local scale. We observe that seasonal biases between active and passive microwave algorithms arise from their different sensitivities to mixed volumetric (sea ice) and surface (ocean) scattering signatures. Sea ice species with mixed signatures include new ice formed during the growth season, and low concentration and water saturated sea ice types that prevail at the Arctic edge during the melt season and the Antarctic edge all year round. In the wintertime, the new QuikSCAT algorithm features an average sea ice edge concentration of 10-15% relative to AMSR-E, improving over previous scatterometer methods in terms of thin ice detection. In the summertime, the ability of the new QuikSCAT algorithm to capture diffuse sea ice conditions is unparalleled, revealing the extent of seasonal errors present in passive microwave algorithms. AMSR-E appears to underestimate the Arctic sea ice extent by up to 15% during the spring and summer months, an error that can be attributed to the sensitivity of sea ice thermal emissions to surface wetting. QuikSCAT provides information that could be used together with passive microwaves to improve the characterization of sea ice in difficult melting conditions. The new QuikSCAT algorithm provides a conservative definition of sea ice edge, more in line with that provided by ship observations and well-suited for applications (such as satellite ocean wind or skin temperature retrievals) that require a reliable masking of sea ice all year round. The only potential source of error in the new QuikSCAT algorithm concerns the episodic appearance of heavy rain structures, which are easily identifiable and otherwise kept at a minimum.

For future work, the GMF based sea ice detection algorithm could be adapted to the Indian Ku-band dual-polarization Oceansat-2 scatterometer with minimum effort. A sea ice detection algorithm for the C-band ASCAT scatterometer on MetOp is already under development following a similar approach tested on ERS satellites [24]. Misclassification due to rain is less of a problem at C-band, but the effective discrimination between sea ice and wind more dependent on across-track location for fan beam scatterometers. We also envision the reprocessing of the entire QuikSCAT data record back to 1999 and a critical comparison against the passive microwave and future ASCAT sea ice extent records.

ACKNOWLEDGMENTS

The authors would like to thank Jeroen Verspeek, Jur Vogelzang and Anton Verhoef for their invaluable assistance in the development of this activity.

REFERENCES

- [1] Fetterer, F., Knowles, K., Meier, M., Savoie, M., "Sea Ice Index. Boulder, CO: National Snow and Ice Data Center". Digital media. 2002. Updated 2009.
- [2] Cavalieri, D.J., Parkinson, C.L., Gloersen, P., Comiso, J.C., Zwally, H.J., "Deriving long term time series of sea ice cover from satellite passive microwave multisensor datasets", *J. Geophys. Res.*, Vol. 104, No. C7, pp. 15803-15814, 1999.
- [3] Remund, Q.P., Long, D.G., "Sea ice extent mapping using Ku-band scatterometer data", *J. Geophys. Res.*, Vol. 104, No. C5, pp. 11515-11527, 1999.
- [4] Anderson, H.S., Long, D.G., "Sea ice mapping method for Seawinds", *IEEE Trans. Geosci. Remote Sens.*, Vol. 43(3), 2005.
- [5] Breivik, L.A., Eastwood, S., "Development of a sea ice type product based on the use of QuikSCAT data", Norwegian Meteorology Institute, MERSEA Report, <http://saf.met.no/docs>, 2006.
- [6] Meier, W., Stroeve, J., "Comparison of sea ice extent and ice-edge location estimates from passive microwave and enhanced resolution scatterometer data", *Ann. Glaciology*, No. 48, pp. 65-70, 2008.
- [7] Abreu, R.D., Wilson, K., Arnett, M., Langlois, D., "Evaluating the use of QuikSCAT data for operational sea ice monitoring", *IEEE IGARSS*, Vol.5, pp. 3032 – 3033, 2002.
- [8] Markus, T., Dokken, S., "Evaluation of late summer passive microwave sea ice retrievals", *IEEE Trans. Geosci. Remote Sens.*, Vol.40(2), 2002.
- [9] Stoffelen, A., "Scatterometry", PhD Thesis, U. Utrecht, pp. II-17, 1998.
- [10] Wentz, F.J., Smith, D.K., "A model function for the normalized cross-section at 14 GHz derived from NSCAT observations", *J. Geophys. Res.*, Vol. 104, C5, pp. 11499-11514, 1999.
- [11] Belmonte Rivas, M., Stoffelen, A., "Near Real-Time sea ice discrimination using SeaWinds on QuikSCAT", OSI SAF Visiting Scientist Report, SAF/OSI/CDOP/KNMI/TEC/TN/168, 2009.
- [12] Spencer, M.W., Wu, C., Long, D.G., "Improved resolution backscatter measurements with the SeaWinds Pencil-Beam Scatterometer", *IEEE Trans. Geosci. Remote Sens.*, 38(1), 2000.
- [13] Stoffelen, A., Portabella, M., "On Bayesian scatterometer wind inversion", *IEEE Trans. Geosci. Remote Sens.*, Vol. 44(6):1523-1533, 2006.
- [14] Portabella, M., Stoffelen, A., "Scatterometer backscatter uncertainty due to wind variability", *IEEE Trans. Geosci. Remote Sens.*, Vol. 44(11): 3356-3362, 2006.
- [15] Leidner, S.M., Hoffman, R.N., Augenbaum, J., "SeaWinds Scatterometer Real-Time BUFR Geophysical Data Product, User's Guide", Version 2.3.0, NOAA/NESDIS, 2000.
- [16] Markus, T., Cavalieri, D.J., "An enhancement of the NASA Team sea ice algorithm", *IEEE Trans. Geosci. Remote Sens.*, Vol. 38(3): 1387-1398, 2000.
- [17] Comiso, J.C., Cavalieri, D.J., Markus, T., "Sea ice concentration, ice temperature and snow depth using AMSR-E data", *IEEE Trans. Geosci. Remote Sens.*, Vol. 41(2): 243-252, 2003.
- [18] Cavalieri, D., and J. Comiso, "AMSR-E/Aqua Daily L3 12.5 km Tb, Sea Ice Conc., & Snow Depth Polar Grids V001", March to June 2004. Boulder, CO, USA: National Snow and Ice Data Center. Digital media, 2004.
- [19] Nie, C., Long, D.G., "A C-band wind/rain backscatter model", *IEEE Trans. Geosci. Remote Sens.*, Vol. 45(3): 621-631, 2007.
- [20] Haarpaintner, J., Tonboe, R.T., Long, D.G., VanWoert, M.L., "Automatic detection and validity of the sea ice edge: an application of enhanced resolution QuikSCAT/SeaWinds data", *IEEE Trans. Geosci. Remote Sens.*, Vol. 42(7): 1433-1443, 2004.
- [21] Heinrichs, J.F., Cavalieri, D.J., Markus, T., "Assessment of the AMSR sea ice concentration product at the ice edge using RADARSAT-1 and MODIS images", *IEEE Trans. Geosci. Remote Sens.*, Vol.44(11), 2006.
- [22] Riggs, G.A., Hall, D.K., Ackerman, S.A., "Sea ice extent and classification mapping with the Moderate Resolution Imaging Spectroradiometer airborne simulator", *Remote Sens. Environ.*, 68:152-163, 1999.
- [23] Worby, A.P., Comiso, J.C., "Studies of the Antarctic sea ice edge and ice extent from satellite and ship observations", *Remote Sens. Environ.*, No. 92: 98-111, 2004.
- [24] Stoffelen, A., "Scatterometer applications in the European Seas" in *Remote Sensing of the European Seas*, V. Barale and M. Gade (Eds.), Springer Netherlands, pp. 269-282, 2008.